A Multifrequency EPR Study on Organic-Capped Anatase TiO_2 Nanocrystals

M. Fittipaldi,*,† M. L. Curri,‡ R. Comparelli,‡ M. Striccoli,‡ A. Agostiano,‡,§ N. Grassi,|| C. Sangregorio,† and D. Gatteschi†

INSTM and Dipartimento di Chimica, Università di Firenze, via della Lastruccia 3, 50019 Sesto Fiorentino (Firenze), Italy, CNR-IPCF Sez. Bari c/o Dipartimento di Chimica, Università di Bari, via Orabona 4, 70126 Bari, Italy, Dipartimento di Fisica, Università di Firenze and INFN, Sezione di Firenze, via G. Sansone 1, 50019 Sesto Fiorentino (Firenze), Italy

Received: December 18, 2008; Revised Manuscript Received: February 6, 2009

A multifrequency electron paramagnetic resonance, EPR, study has been carried out on TiO_2 nanocrystals (NCs) capped by organic moieties prepared according to both a nonhydrolytic and a hydrolytic procedure, respectively, with spherical or rodlike shape. In particular, EPR measurements have been performed in the 9−95 GHz range, at various temperatures, and with and without UV irradiation. The behavior of the electrons promoted in the conduction band by UV irradiation and of the holes in the valence band has been monitored by means of the generated paramagnetic species that are detectable by EPR, thus enabling the identification of the different sites at which the charges are trapped. In particular, an EPR signal which can be considered a mark of the localization of the photoinduced charge on a carbon of the capping molecule is observed. The presence of paramagnetic species on the surfaces of TiO_2 NCs has been used to account for the catalytic performance of such a class of nanostructured material which has been recently proven to present a high catalytic efficiency. The observed carbon radical is suggested to be responsible for the higher catalytic activity of organic capped nanosized catalysts. Indeed, upon irradiation, the intensity of this signal with respect to the bulk Ti^{3+} signal is larger in the NCs characterized by higher photocatalytic activity; namely, those prepared with a hydrolytic procedure.

Introduction

Nanostructured materials are attracting growing attention, both for fundamental research[1,2] and for their unique properties, different from those found in bulk materials. In particular, wide band gap titania nanocrystals, NCs, are investigated for their remarkable properties in several applications, such as solar cells,[3] photocatalysts for water photolysis,[4] and degradation of environmental pollutants in air and waste water.[5] These applications are extremely relevant for both environment maintenance and for clean, secure, and renewable energy source. The very high surface-to-volume ratio in small TiO_2 particles favors photoreaction rates, because it facilitates reaction/interaction with the substrate. The increase in the band gap energy with decreasing NP size can possibly enhance the redox potential of the electron−hole pairs.[6,7] Such an effect, however, results in a reduced effectiveness to sunlight activation for smaller sized NCs. As a consequence, there exists an optimal size for a given photocatalytic reaction. The recombination rate of the electron−hole pairs is also dependent on the size and shape of the NCs. Such a recombination rate is faster in larger particles, for which the recombination occurs in the core, and can be reduced by decreasing the NC size. However, a further reduction in the NC size increases the rate of the process, since the surface recombination processes become predominant.[8]

The design of TiO_2 NCs with specific properties is achieved also via a proper tuning of the NC surface chemistry. Chemical synthetic routes able to control NC size and shape and, accordingly, their physical and chemical properties, can usefully take advantage by use of organic molecules that are able to direct the NC growth, preventing aggregation, through the coordination of the NC surface.[9]

The electron−hole (e^-/h^+) pairs, generated by over-band-gap photoirradiation, can be trapped at the Ti site, at the surface oxygen or, when present, on the capping organic molecules on TiO_2 NC surface. The photogenerated surface radicals act as reactive species in the catalytic processes: the trapped charge can be transferred from the surface radical to the substrate at the surface of the NCs for the initiation of the photocatalytic reaction. EPR provides the possibility of identifying reactive paramagnetic species by their distinctive Hamiltonian parameters and of deepening the understanding of the reaction mechanisms of the photocatalyst and has been widely used on TiO_2.[10−12] Howe and Grätzel[10] reported the EPR spectra of electrons trapped on Ti^{4+} sites formed on irradiation of colloidal TiO_2 solutions and characterized the electronic structure of the resulting Ti^{3+} centers. Adsorbed O_2 behaves as a very efficient electron scavenger, and indeed, traces of O_2 are sufficient to inhibit formation of Ti^{3+}.[11,13] On the other hand, the interpretation of the EPR spectra observed for the photogenerated hole trapped species is complicated due to the less distinctive markers for the relevant species. This is reflected in the fact that different EPR signals have been observed, depending on the adopted preparation procedure.[10−12,14,15]

Some of us recently reported the photocatalytic investigation of anatase TiO_2 NCs of different shapes; namely, nanorods (NRs, diameter about 3 nm and length about 20 nm) and nanodots (NDs, mean particle size, 6 nm), capped with different molecules, oleic acid (OLEA) and tri-*n*-octylphosphine oxide (TOPO).[16,17] The NCs have been synthesized by means of

* Corresponding author. E-mail: maria.fittipaldi@unifi.it.
† Dipartimento di Chimica, Università di Firenze and INSTM.
‡ CNR-IPCF Sez. Bari.
§ Dipartimento di Chimica, Università di Bari.
|| Dipartimento di Fisica, Università di Firenze and INFN.

10.1021/jp8111765 CCC: $40.75
Published on Web 03/20/2009

distinct synthetic routes, thus turning out in different properties, mainly concerning the surface status of the NCs. In particular, a hydrolytic reaction has been used for the OLEA−TiO_2 NCs and a nonhydrolytic for the TOPO−TiO_2 NCs. The two resulting differently capped TiO_2 NCs differ for the steric hindrance of the passivating ligand and for the nature of the functional group binding to the crystal surface; that is, either $-CO_2^-$ or −P═O, respectively. In the previous study of the photocatalytic activity of the OLEA- and the TOPO-capped TiO_2 NCs in the degradation of an organic model compound, despite their comparable size, a much higher efficiency of the former NC type has been demonstrated. In addition, the photocatalytic activity of OLEA−TiO_2 NCs has been demonstrated to be even higher than that achieved by the commercial TiO_2 P25 Degussa,[9] a typical standard for photocatalytic reactions, despite the naked surface of the commercial catalyst. This behavior indicates a direct involvement of the interface of material in the photocatalytic reactions.

To elucidate the structural and electronic properties directing the photo reactivity of the catalytic compounds, we investigated the photogenerated reactive species in the differently capped TiO_2 NCs by multifrequency EPR spectroscopy in the range 9−95 GHz. The EPR results are discussed in relation to the photocatalytic activity of the investigated systems.[9] From this correlation, some new insights into the electron transfer processes are obtained which could be possibly extended to other systems, such as C-doped TiO_2 and DSC, dye-sensitized solar cells.

Moreover, in the investigated systems, the recombination kinetics are very fast, of the order of picoseconds.[18−20] Enhanced charge separation can be achieved in surface-modified TiO_2 NCs[21] due to the instantaneous separation of the charge pairs, with the holes on the donating organic modifier and the electron in the conduction band of TiO_2. The transient species involved in the early stages of charge pair formation can be followed by time-resolved EPR.[22] The EPR data reported in this work suggest the sensitiveness of the continuous wave EPR spectra acquired at high-field and high-frequency to the kinetic of the trapped charges in organic capped TiO_2 NCs. The obtained results provide original insight for the comprehension of the photocatalytic activity of organic capped nanostructured catalysts.

Methods

Materials. Commercial TiO_2 P25 NCs were purchased by Degussa (nonporous anatase; surface area, 50 $m^2\ g^{-1}$; mean diameter, approximately 30 nm). *n*-Heptadecane (C_7H_{16} or HD, 99%), titanium tetrachloride ($TiCl_4$, 99%), titanium tetraisopropoxide ($Ti(OPri)_4$ or TTIP, 98.9%), tri-*n*-octyl-phosphineoxide ($(C_8H_{17})_3PO$ or TOPO, 90%), trimethylamino-*N*-oxide dihydrate or anhydrous ($(CH_3)_3NO_2H_2O$ or TMAO, 98%), oleic acid ($C_{18}H_{33}CO_2H$ or OLEA, 90%), ethylene glycol ($C_2H_4(OH)_2$ or EG, 98%) were purchased from Aldrich.

Chloroform and methanol were of the highest purity available and purchased from Aldrich. Twice distilled water was used.

Synthesis of TiO_2 NCs. The synthesis of TiO_2 NCs was performed by using standard airless techniques as already reported elsewhere.[16,17] Briefly, hydrolytic TiO_2 nanorods (OLEA−TiO_2 NR) have been prepared by adding TTIP to previously degassed oleic acid under nitrogen flow at 100 °C. The anhydrous environment prevents TTIP from premature hydrolysis. The subsequent injection of an aqueous solution of trimethylamine-*N*-oxide (TMAO) dihydrate starts the fast hydrolysis, which leads to the formation of OLEA-capped anatase TiO_2 NRs, (average size 3−20 nm, as confirmed by TEM measurements).

Conversely, nearly spherical anatase TiO_2 NCs (OLEA−TiO_2 ND, sizing about 6 nm, as measured by TEM analysis) have been obtained by the slow hydrolysis of TTIP. In this case, TTIP has been added to previously dried OLEA containing anhydrous TMAO and ethylene glycol under nitrogen flow. The TTIP hydrolysis occurs upon reaction with water realized during the esterification reaction of EG with OLEA.

Finally, nonhydrolytic anatase TOPO-capped TiO_2 nanodots (TOPO−TiO_2 NDs, diameter 6 nm) were obtained by reacting $TiCl_4$ and TTIP at 300 °C in a mixture of heptadecane and tri-*n*-octylphosphine oxide (TOPO) in an anhydrous environment.

Irrespective of the synthetic route, the obtained NCs were precipitated from the reaction mixture by adding methanol (or ethanol) and isolated by centrifuge. The collected powders were washed three times and dried 24 h under vacuum for EPR and PIXE measurements.

FTIR Characterization. The characterization of the NCs was performed by FT-IR. Spectra of TiO_2 NC powders were collected with a Perkin-Elmer Spectrum GX FT-IR spectrometer with a resolution of 4 cm^{-1}. Measurements were performed by diluting the samples in pressed KBr pellets.

EPR Characterization. The X-band and W-band cw EPR measurements were performed by using the 9 and 95 GHz Bruker Elexys E500 instrument (Bruker, Rheinstetten, Germany). An Oxford Instruments ESR 900 continuous He flow cryostat and a Bruker continuous N_2 flow cryostat (ER4131VT) were used to obtain low temperatures. The frequency of the field modulation was 100 kHz. The power, temperature, and field modulation at which the spectra were acquired are specified in the figure captions.

The UV irradiation was realized using a 75 W xenon lamp and an optical fiber to guide the radiation to the sample. The fiber was inserted in the EPR tube for the X-band measurements and was in contact with the top-end of the 95 GHz tube for the W-band measurements.[23]

For the X-band EPR measurements in vacuo, the sample was evacuated such that a residual pressure of 10^{-5} mbar was present in the EPR tube, subsequently sealed. For the measurements of this sample, a slit-open resonator was used (Bruker ER 4102ST) to irradiate the sample. The simulations of the EPR spectra were performed using the EasySpin Matlab toolbox programmed for EPR simulations[24] (free download at www.easyspin.org). The intensity of the W-band EPR signal was calculated taking into account the quantities that change by varying the temperature: the power at which the spectra have to be acquired, the line width of the signal, the merit factor of the resonator. The area of the signal was estimated as the product of the signal intensity times the line width squared.

Results

The surface of the as prepared TiO_2 NCs, capped with OLEA and TOPO, was characterized by FT-IR spectra. The TOPO−TiO_2 NCs (Figure 1A) show the typical antisymmetric and symmetric C−H stretches (2920−2850 cm^{-1}). The weak stretch at 1240 cm^{-1} can be ascribed to the −P═O moiety involved in the coordination with the surface, thus confirming the presence of a TOPO layer on the TOPO−TiO_2 surface. The IR spectra of OLEA−TiO_2 (irrespective of the shape) show the presence of C−H stretch vibrations (both antisymmetric and symmetric) at 2920−2850 cm^{-1} and the presence of a typical olefinic ═C−H stretch (Figure 1B). The two intense bands at 1520 and 1436 cm^{-1} can be ascribed to the antisymmetric and

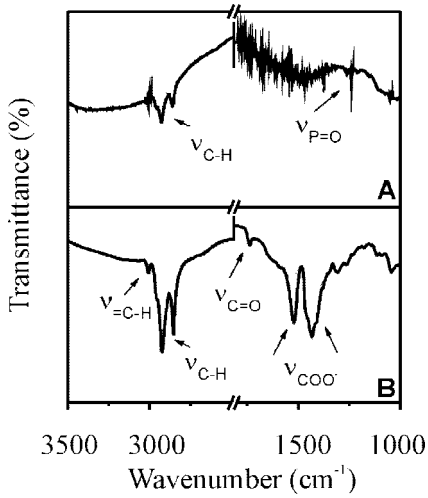

Figure 1. FT-IR spectra in the 3500−1000 cm^{-1} region of TiO_2 NCs. (A) TOPO−TiO_2, (B) OLEA−TiO_2 NCs.

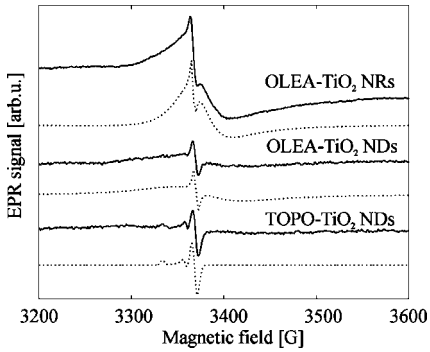

Figure 2. RT X-band EPR spectra of TOPO−TiO_2 NDs, OLEA−TiO_2 NDs, and OLEA−TiO_2 NRs. The EPR spectra have been acquired using 2 G of modulation amplitude and a microwave power of 2 mW. Dotted lines: simulations of the EPR spectra.

symmetric vibrations of carboxylate anions that form a complex with the surface Ti centers. Moreover, the weakness of the C═O stretching suggests its involvement in H-bonding with a Ti−OH_2^+ surface group, as reported by Comparelli et al. (see ref 9 and references therein).

The X-band spectra at low temperature of all the NCs reveal a signal at $g = 4.3$ that is attributed to the ubiquitary Fe^{3+} in low symmetry environment (see Figure S1 of the Supporting Information). The intensity of this signal is characteristic of the defined NCs, being higher for the OLEA−TiO_2 NDs than for the OLEA−TiO_2 NRs. No apparent change in the Fe signal is observed upon UV illuminations; therefore, the involvement of Fe impurities in the photocatalytic process can be excluded, at least in relation to the time-scale of the X-band experiments.

A characterization of the impurities present in the NCs also for species that are EPR-silent has been obtained by PIXE analysis (details in Supporting Information).

In the OLEA-TiO_2 NRs, without illumination at room temperature (RT), two EPR signals are present around $g = 2$ (Figure 2). Of these two signals, one is sharp, $\Delta H_{pp} = 6.9$ G, and isotropic, with $g = 2.0037$ (hereafter referred to as signal A), and the other is broad, $\Delta H_{pp} \sim 46$ G, with a g value of 2.000, (signal B, Table 1). Both of them increase upon a decrease in the temperature. In Figure 2, the simulation of the observed EPR species is also shown. Signal A has been simulated using a Lorentzian line shape, whereas a good simulation of signal B was achieved only using a Dysonian line shape.

TABLE 1: g Values of the Paramagnetic Species in TiO_2 Particles

species	g_{xx}	g_{yy}	g_{zz}
A	2.003	2.003	2.003
B	2.000	2.000	2.000
C	2.025	2.009	2.003
D	1.989	1.989	1.958
$(O_2^-)^a$	2.025	2.009	2.003
$(O^-)^a$	2.016	2.012	2.002

[a] From Howe and Grätzel.[11]

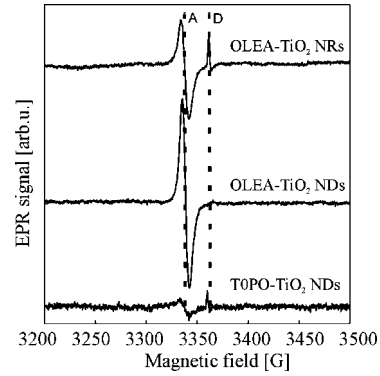

Figure 3. X-band EPR signals of the TiO_2 NCs obtained as the difference between the spectrum acquired with the xenon lamp on and that without irradiation. The EPR spectra were acquired at $T = 40$ K, using 2 G of modulation amplitude and a microwave power of 6.5 μW. Dashed lines indicate the resonance field of signal A and of the perpendicular component of signal D.

For OLEA−TiO_2 NDs, at RT, the A and B signals are also observed around $g = 2$: A has $\Delta H_{pp} = 6.5$ G and B has $\Delta H_{pp} \sim 70$ G and very low intensity (Figure 2). For TOPO−TiO_2 NDs, beyond the sharp signal at $g = 2.003$ (A, $\Delta H_{pp} = 6$ G), an anisotropic signal (hereafter referred to as C, Table 1) with g values of 2.0247, 2.0097, and 2.003 is observed (Figure 2). The commercial TiO_2 Degussa P25 does not show any EPR signal at RT.

Summarizing, signal A is present in all the investigated NC types in the dark, although different intensities and line widths have been recorded. The A and B signals which we observe at RT for OLEA−TiO_2 NCs are very similar in shape to those reported by Nakamura et al.[25] for plasma-treated TiO_2 powders.

The changes in the EPR spectra of the different samples induced by light excitation are shown in Figure 3, as obtained at 40 K by subtracting the spectra recorded upon light excitation from those recorded in the dark.

In the OLEA−TiO_2 NRs, upon UV excitation at low temperature, a sharp axial signal (D) appears (see Figure 3 and Table 1) with $g_{xx} = g_{yy} = 1.989$ and $g_{zz} = 1.958$. Moreover, the intensity of signal A increases. Both signals are induced by UV irradiation in the presence of oxygen under atmospheric pressure. The same signals are observed when the sample is irradiated in vacuo at 40 K (see the Methods Section).

UV excitation of OLEA−TiO_2 NDs generates an increase in signal A, whereas signal D is almost not detectable (Figure 3). UV excitation of TOPO−TiO_2 NDs at 40 K induces an increase in signal A, and signal D appears.

The signal A-to-signal D intensity ratio for the different NCs was estimated. This ratio is the highest for the OLEA−TiO_2 NDs (40) and is the lowest for the TOPO−TiO_2 NDs (1), whereas it is 3 for the OLEA−TiO_2 NRs (see Table S2 in the Supporting Information).

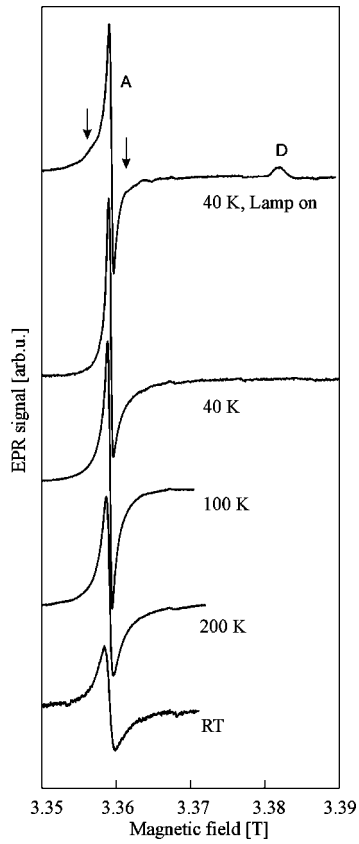

Figure 4. W-band EPR spectra of OLEA−TiO_2 NR at various temperatures and spectrum acquired at 40 K under UV irradiation.

For OLEA−TiO_2 NRs at RT, a signal is observed at W-band (Figure 4), which is not perfectly symmetric. The simulation gives good agreement with the experimental spectrum using a g value of 2.0033, from which assignment is made to signal A, $\Delta H_{PP} = 14.5$ G. The broad signal B observed at X-band underneath signal A is almost completely lost in W-band. Most probably, this is caused by a further broadening due to the increased field. The asymmetry of signal A can derive from a remaining contribution of signal B. Nevertheless, the temperature dependence of the line width of signal A can be followed very well at this frequency due to the fact that signal B has a very low intensity and is shifted to higher magnetic fields.

The line width of signal A decreases remarkably upon lowering the temperature (see Figure 4 and S2 of the Supporting Information). It has to be noted that a signal at $g = 2.003$ and $\Delta H_{PP} = 14$ G has been also observed at Q-band at RT (data not shown).

At 40 K, upon irradiation of the sample with a xenon lamp, signal A does not change in the peak-to-peak intensity, but unresolved side signals appear (indicated by arrows in Figure 4) that have the same g value but with a larger line width. On the basis of the g value, this signal could be attributed to a species somehow related to species A, although not identical. Moreover, the perpendicular component of D at $g = 1.989$ appears (Figure 4). The parallel component of this signal is not observed in W-band due to its increased line width and low intensity.

The RT W-band EPR spectrum of OLEA−TiO_2 NDs is quite similar to that of NRs, (Figure 5). The corresponding line width is 14 G for OLEA−TiO_2 NRs and 20 G for OLEA−TiO_2 NDs. This signal is not observed for TOPO−TiO_2 NDs, although it is present at the X band.

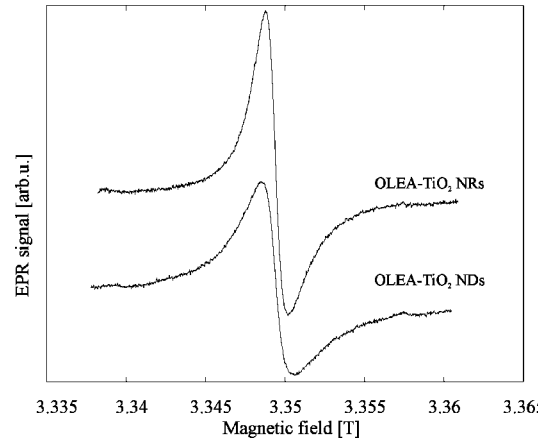

Figure 5. RT W-band EPR spectra of OLEA−TiO_2 NRs and OLEA−TiO_2 NDs. The EPR spectra have been acquired using 2 G of modulation amplitude and a microwave power of 0.05 mW.

Discussion

Distinct behavior of the EPR signals is observed for the different types of analyzed NCs, both in the dark and under illumination. The increased spectral resolution of the W-band EPR spectra allows the separation of signals A and B and the possibility to properly follow the line width dependence of signal A on the temperature and, therefore, to characterize this signal more finely.

Moreover, the understanding of the relation between the surface chemistry and the EPR signals observed at X-band is more straightforward from the comparison of the signals that are photoinduced. These data could also give insight into the specific photocatalytic activity of the organic-modified TiO_2 NCs, thus accounting for the remarkable efficiency demonstrated for OLEA−TiO_2 NDs and NRs.

In many cases, the assignment of the signals can be done by comparison with spectra reported in the literature. In fact, signal C corresponds to the superoxide radical. In TiO_2 semiconductors, g values larger than g_e have generally been attributed to hole centers at the semiconductor surface stabilized by electrostatic interaction with electrons trapped by O_2 molecules adsorbed at the surface of the NCs, therefore referred to as oxygen-related sites.[10,14] These sites are characterized by anisotropic **g** tensors. The unpaired electron of the superoxide species, O_2^- ion, is confined in a π-type orbital, and its EPR spectrum is intrinsically orthorhombic[14] (see also Table 1).

Signal B, with g values lower than g_e, could be tentatively attributed to free electrons in the conduction band.[13] This assignment is reinforced from the Dysonian character of the line shape.

Signal D is observed upon illumination with different intensities in all the three investigated NCs. The g values of signal D, smaller than g_e, are typical of trapped electrons at the Ti sites ($Ti^{4+} + e^- \rightarrow Ti^{3+}$). In particular, this signal, which we observe also in the presence of O_2 and with a quite sharp line shape (in X-band), has been found to be characteristic of species in which the unpaired electron occupies the d-orbital of lattice Ti atoms.[21] The signal is observed also at W-band, but it is much broader, in such a way that only the perpendicular feature is resolved. At higher frequencies, the enhanced line width is most probably due to g strain effects. No EPR signal associated with the surface sites is observed (surface Ti centers: $g_\perp = 1.924$, $g_{||} = 1.885$).[22] This evidence is consistent with the coordinating effect of the capping molecules, which are able to passivate surface defects, thus removing trapping sites.

Signal A is observed in all the investigated NCs, therefore pointing out that the same trapping site is generated independently of the different analyzed capping. A relevant feature is that the signal is symmetric also at W-band, thus putting an upper limit to possible anisotropies on the g values. In X-band, Li et al. [26] have observed a similar isotropic signal in the dark at RT and at low temperature upon illumination in C-doped titania. In addition, Nakamura et al. (see ref 25 and refs therein) have reported an isotropic signal observed at RT. As already mentioned, a superoxide species would give an orthorhombic EPR signal;[14] the same would happen for an O^- species (see O^- g values in Table 1). Signal A strongly resembles that reported by Rajh et al.[22] in capped titania NCs at $g = 2.004$ who attributed it to photogenerated holes localized on carbon-centered π-orbitals of the capping molecules. The line width dependence on the capping ligand has been observed, analogously to what is here reported, thus pointing out the surface character of this species. Additionally a dependence of the line width on the shape of the NCs (see Figure 2 and 5) is detected. Howe and Grätzel[10] observed an "unusual" four-line signal centered on $g = 2.002$ (intensity ratio 1:3:3:1, splitting 23 G) for TiO_2 in acetate solution irradiated at 77 K and attributed it to methyl radicals.

From these considerations, we assign signal A to holes localized at the surface of the NCs on the capping molecules. The small difference in the A signal between OLEA and TOPO derivatives and the comparison with the Howe et al. data suggest a hole localized on the aliphatic chains. Notably, $-CO_2^-$ is the surfactant binding group to the crystal surface in OLEA$-TiO_2$ in which this hole-related signal grows most upon irradiation: the C atoms of the TOPO molecules are less close to the interface TiO_2/capping molecule. Extending the path of the photogenerated charges increases the probability of recombination processes, and in principle, this provides a further support to the assignment. Notably, in DSC, the optical transition has a metal-to-ligand charge transfer character: excitation of the dye involves transfer of an electron from the metal to the π^* orbital of the surface anchoring carboxylated bipyridyl ligand (when carboxylate is the binding group) from where it is injected to the conduction band of TiO_2.[27,28] Signal A can be considered as a mark of the localization of the charge on a carbon of the capping molecule. A similar signal is observed also when C is a contaminant of the TiO_2.[29]

Moreover, the presence of the signal A in the dark for all the three samples is consistent with the presence of acceptor levels above the valence band such that electrons can be promoted by thermal energy. These electrons may subsequently be trapped and therefore be visible also when the temperature is lowered. The acceptor levels could derive from the carbon atoms of the organic surfactants. It is necessary to recal the nanocrystalline character of these samples and, therefore, the huge influence of the surface chemical state on their electronic structure. Further support for this interpretation is provided by theoretical investigations on C-doped TiO_2 systems. These studies have shown that C-doping of TiO_2 introduces states just above the valence band of pure TiO_2,[30] assigned as carbon 2p states.[30,31] Moreover, it has been found that for a high carbon concentration, the valence band edge is quite delocalized, with significant overlap between the carbon 2p states and oxygen 2p states.[30] This would result in a high hole mobility,[30] which is a prerequisite for a strong oxidation power.

It is worth noting that in our capped NCs, the UV irradiation generates holes localized on C atoms, whereas oxygen-related sites are absent. This gives a clear indication of the relative energy levels of the possible trapping sites.

A comparison of the spectra in Figure 3 reveals that upon irradiation, the surface hole-trapped radical signal, compared with the Ti^{3+} signal, grows more in the OLEA$-TiO_2$ NCs than in the TOPO$-TiO_2$ NDs, which can be explained by the more extended path of the photogenerated charges prior trapping for TOPO$-TiO_2$ NDs. The trend observed by EPR measurements is in good agreement with the photocatalytic activity that is higher in OLEA$-TiO_2$ NCs than in TOPO$-TiO_2$ NDs. The photocatalytic efficiency of OLEA$-TiO_2$ NCs, evaluated as the percentage of decoloration of MeRed absorbance at $\lambda_{max} = 520$ nm, after 30 min was found to be 2 times larger than for TOPO$-TiO_2$ NDs (see Figure S3 of the Supporting Information).[9] This is clearly not related to the shape of the NCs, but to the capping molecules. To compare the two sets of data, we have to remember that although the photocatalytic characterization had been carried out in a water solution, the EPR measurements were performed on powders. Thus, the latter provide unique information on the charge separation prior to charge transfer to solvent molecules and explain their distinctive photocalytic activity. Indeed, since the catalytic activity proceeds through surface radicals, the EPR data reveal that a larger amount of surface radicals, as compared to lattice Ti^{3+} centers, is generated upon irradiation in the OLEA$-$NCs, as compared to the TOPO$-$NDs.

Despite the different content of Fe impurity in the OLEA$-TiO_2$ NRs and OLEA$-TiO_2$ NDs (Table 1), their catalytic activity is approximately the same[32] (see Figure S3 of the Supporting Information). It has to be noted that the Fe content can affect the electron$-$hole recombination rates, and indeed, transition-metal-doped TiO_2 suffers from an increase in recombination centers introduced by the dopant-related localized d states deep in the band gap of TiO_2.[33] Remarkably, the highest A/D signal intensity ratio exhibited by OLEA$-TiO_2$ NDs is consistent with the observed higher photocatalytic activity (i.e., a larger number of surface radicals) than the corresponding NRs. However, this potential higher photocatalytic activity is counterbalanced by the larger amount of Fe impurity present (i.e., the larger number of recombination centers) in the OLEA$-TiO_2$ NDs as compared to the corresponding NRs. Although more surface radicals are produced in OLEA$-TiO_2$ NDs as compared to NRs, their recombination rates could be faster compared to NRs, from which a comparable photocatalytic activity would result for OLEA$-TiO_2$ NDs and NRs.

In conclusion, in powder samples of the analyzed organic-modified TiO_2, the hole trapping site is a carbon-centered radical. The formation of such a carbon radical could in some way stabilize the excited state of OLEA-TiO_2 because its generation would involve the trapping of TiO_2 holes.[21] Thus, the charge pair would be instantaneously spatially separated (the hole on the donating capping ligand and the electron in the conduction band of the semiconductor). Such a charge separation would allow a higher lifetime of the photogenerated charges,[34] thus enhancing the probability of OH radical generation in water matrixes, which are known to be responsible for the target compound degradation.[35]

The line width of signal A observed in the dark in W-band in OLEA$-TiO_2$ NRs is approximately the same as that obtained in Q-band and larger compared to that obtained in X-band. This behavior suggests that the increase in the line width on going to microwave frequency larger than that of the X-band is not only due to g-strain. Instead, it could be due to the different time windows characteristic of the spectrometers employed. Spectrometers operating at higher frequencies are sensitive to

faster dynamics and, therefore, to charge carriers with more delocalized character, which would consequently have a larger line width.

The W-band spectra show a notable decrease in the line width of signal A by lowering the temperature (Figures 2 and 4). This indicates that the RT line width is dominated neither by unresolved hyperfine interaction nor by dipolar interaction between paramagnetic centers, since these interactions are not expected to decrease on going to lower temperatures. The line width behavior could be dominated by the trapped electron−hole recombination time, which is expected to increase by lowering the temperature, and as a result, the line width would decrease, in agreement with the observed experimental trend. The trapped electron−hole recombination time are intimately related to the mobility of the charges,[36] which is also expected to decrease upon lowering the temperature, giving rise to more localized species. If our interpretation is correct, the temperature dependence of the EPR line width of the radicals in these systems can also provide a very useful test for models of electron- and hole-trapping mechanisms, since the temperature dependence of transient absorption data is generally more difficult to acquire on these samples.[37]

Concluding Remarks. In conclusion, the nature of the trapping sites in organic-capped colloidal TiO_2 NCs is inferred from the experimental evidence reported, which has been analyzed and discussed considering the surface chemical state and EPR data already reported in the literature. The analysis of the spectra is simplified by the use of a multifrequency EPR approach.

Moreover, at high frequency, evidence of the sensitivity of the EPR spectral features to the mobility of charge carriers has been collected.

The EPR results are able to account for the trends of photocatalytic efficiency recorded for the differently surface-modified NCs, in line with the high catalytic efficiency of such a class of nanostructured materials. We believe that our results are very important for the synthesis and designing of new photoactive catalysts with tailored surface chemistry.

Acknowledgment. Dr. C. Innocenti (University of Firenze) is kindly acknowledged for helpful discussions. Ministero dell'Istruzione, dell'Università e della Ricerca (MIUR) is gratefully acknowledged for financial support to M. Fittipaldi. This work has been supported in part by the EC-funded Project NOVOPOLY (Contract no. STRP 013619) and by Apulia Region within the Scientific Research Framework Program 2006 (Contract no. PE049).

Supporting Information Available: PIXE, photocatlytic characterization, and Supporting Information for the EPR data on the NCs. This information is available free of charge via the Internet at http://pubs.acs.org.

References and Notes

(1) Nalwa, H. S. *Handbook of Nanostructured Materials and Nanotechnology*, Academic Press: New York: 2000.

(2) Thiaville, A.; Miltat, J. *Science* **1999**, *284*, 1939–1940.

(3) Tennakone, K.; Jayaweera, P. V. V.; Bandaranayake, P. K. M. *J. Photochem. Photobiol., A* **2003**, *158*, 125–130.

(4) Matsumoto, Y.; Unal, U.; Tanaka, N.; Kudo, A.; Kato, H. *J. Solid State Chem.* **2004**, *177*, 4205–4212.

(5) Ollis, D. F. *Comptes Rendus de l'Academie des Sciences, Series IIC: Chemistry* **2000**, *3*, 405–411.

(6) Wang, C. C.; Zhang, Z. B.; Ying, J. Y. *Nanostruct. Mater.* **1997**, *9*, 583–586.

(7) Bahnemann, D. W. *Isr. J. Chem* **1993**, *33*, 115–136.

(8) Zhang, Z. B.; Wang, C. C.; Zakaria, R.; Ying, J. Y. *J. Phys. Chem. B* **1998**, *102*, 10871–10878.

(9) Comparelli, R.; Fanizza, E.; Curri, M. L.; Cozzoli, P. D.; Mascolo, G.; Passino, R.; Agostiano, A. *Appl. Catal., B* **2005**, *55*, 81–91.

(10) Howe, R. F.; Grätzel, M. *J. Phys. Chem.* **1985**, *89*, 4495–4499.

(11) Howe, R. F.; Grätzel, M. *J. Phys. Chem.* **1987**, *91*, 3906–3909.

(12) Anpo, M.; Shima, T.; Kubokawa, Y. *Chem. Lett.* **1985**, 1799.

(13) Berger, T.; Sterrer, M.; Diwald, O.; Knozinger, E.; Panayotov, D.; Thompson, T. L.; Yates, J. T. *J. Phys. Chem. B* **2005**, *109*, 6061–6068.

(14) Anpo, M.; Che, M.; Fubini, B.; Garrone, E.; Giamello, E.; Paganini, M. C. *Top. Catal.* **1999**, *8*, 189–198.

(15) Kumar, C. P.; Gopal, N. O.; Wang, T. C.; Wong, M. S.; Ke, S. C. *J. Phys. Chem. B* **2006**, *110*, 5223–5229.

(16) Cozzoli, P. D.; Kornowski, A.; Weller, H. *J. Am. Chem. Soc.* **2003**, *125*, 14539–14548.

(17) Trentler, T. J.; Denler, T. E.; Bertone, J. F.; Agrawal, A.; Colvin, V. L. *J. Am. Chem. Soc.* **1999**, *121*, 1613–1614.

(18) Serpone, N.; Lawless, D.; Khairutdinov, R.; Pelizzetti, E. *J. Phys. Chem.* **1995**, *99*, 16655–16661.

(19) Colombo, D. P.; Bowman, R. M. *J. Phys. Chem.* **1996**, *100*, 18445–18449.

(20) Colombo, D. P.; Bowman, R. M. *J. Phys. Chem.* **1995**, *99*, 11752–11756.

(21) Rajh, T.; Nedeljkovic, J. M.; Chen, L. X.; Poluektov, O.; Thurnauer, M. C. *J. Phys. Chem. B* **1999**, *103*, 3515–3519.

(22) Rajh, T.; Poluektov, O.; Dubinski, A. A.; Wiederrecht, G.; Thurnauer, M. C.; Trifunac, A. D. *Chem. Phys. Lett.* **2001**, *344*, 31–39.

(23) Janssen, G.; Bouwen, A.; Casteels, P.; Goovaerts, E. *Rev. Sci. Instrum.* **2001**, *72*, 4295–4296.

(24) Stoll, S.; Schweiger, A. *J. Magn. Reson.* **2006**, 42–55.

(25) Nakamura, I.; Negishi, N.; Kutsuna, S.; Ihara, T.; Sugihara, S.; Takeuchi, K. *J. Mol. Catal., A: Chem.* **2000**, *161*, 205–212.

(26) Li, Y.; Hwang, D. S.; Lee, N. H.; Kim, S. J. *Chem. Phys. Lett.* **2005**, *404*, 25–29.

(27) Grätzel, M. *J. Photochem. Photobiol., C* **2003**, *4*, 145–153.

(28) Benko, G.; Kallioinen, J.; Korppi-Tommola, J. E. I.; Yartsev, A. P.; Sundstrom, V. *J. Am. Chem. Soc.* **2002**, *124*, 489–493.

(29) Fittipaldi, M.; Gombac, V.; Montini, T.; Fornasiero, P.; Graziani, M. *Inorg. Chim. Acta* **2008**, *361*, 3980–3987.

(30) Wang, H.; Lewis, J. P. *J. Phys. Condens. Matter* **2005**, *17*, L209−L213.

(31) DiValentin, C.; Pacchioni, G.; Selloni, A. *Chem. Mater.* **2005**, *17*, 6656–6665.

(32) Cozzoli, P. D.; Comparelli, R.; Fanizza, E.; Curri, M. L.; Agostiano, A. *Mater. Sci. Eng., C* **2003**, *23*, 707–713.

(33) Choi, W. Y.; Termin, A.; Hoffmann, M. R. *J. Phys. Chem.* **1994**, *98*, 13669–13679.

(34) Bedja, I.; Kamat, P. V. *J. Phys. Chem.* **1995**, *99*, 9182–9188.

(35) Hoffmann, M. R.; Martin, S. T.; Choi, W. Y.; Bahnemann, D. W. *Chem. Rev.* **1995**, *95*, 69–96.

(36) Tachikawa, T.; Tojo, S.; Kawai, K.; Endo, M.; Fujitsuka, M.; Ohno, T.; Nishijima, K.; Miyamoto, Z.; Majima, T. *J. Phys. Chem. B* **2004**, *108*, 19299–19306.

(37) Skinner, D. E.; Colombo, D. P.; Cavaleri, J. J.; Bowman, R. M. *J. Phys. Chem.* **1995**, *99*, 7853–7856.

JP8111765